Cardiovascular Research (2016) **112**, 452–463
doi:10.1093/cvr/cvw192

A mutation in the glutamate-rich region of RNA-binding motif protein 20 causes dilated cardiomyopathy through missplicing of titin and impaired Frank–Starling mechanism

Abdelaziz Beqqali[1]*, Ilse A.E. Bollen[2], Torsten B. Rasmussen[3], Maarten M. van den Hoogenhof[1], Hanneke W.M. van Deutekom[1], Sebastian Schafer[4,5], Jan Haas[6,7], Benjamin Meder[6,7], Keld E. Sørensen[3], Ralph J. van Oort[1], Jens Mogensen[8], Norbert Hubner[7,9,10], Esther E. Creemers[1], Jolanda van der Velden[2], and Yigal M. Pinto[1]

[1]Department of Experimental Cardiology, Academic Medical Center, Meibergdreef 15, 1105AZ, Amsterdam, The Netherlands; [2]Department of Physiology, VU University Medical Center, Institute for Cardiovascular Research (ICaR-VU), van der Boechorststraat 7, 1081 BT, Amsterdam, The Netherlands; [3]Department of Cardiology, Aarhus University Hospital, Norrebrogade 44, DK-8000, Aarhus, Denmark; [4]National Heart Research Institute Singapore, National Heart Centre Singapore, 5 Hospital Drive, Singapore 169609, Singapore; [5]Division of Cardiovascular & Metabolic Disorders, Duke-National University of Singapore, 8 College Road, Singapore 169857, Singapore; [6]Department of Internal Medicine III, Cardiology, University Hospital of Heidelberg, 69120 Heidelberg, Germany; [7]DZHK (German Centre for Cardiovascular Research), Oudenarder Straße 16, 13347 Berlin, Germany; [8]Department of Cardiology, Odense University Hospital, Sdr. Boulevard 29, 5000 Odense, Denmark; [9]Charité-Universitätsmedizin, Charitéplatz 1, 10117 Berlin, Germany; and [10]Cardiovascular and Metabolic Sciences, Max-Delbrück-Center for Molecular Medicine (MDC), Robert-Rössle-Str. 10, 13125 Berlin, Germany

Received 25 February 2016; revised 14 July 2016; accepted 21 July 2016; online publish-ahead-of-print 5 August 2016

Time for primary review: 14 days

Aim Mutations in the RS-domain of RNA-binding motif protein 20 (RBM20) have recently been identified to segregate with aggressive forms of familial dilated cardiomyopathy (DCM). Loss of RBM20 in rats results in missplicing of the sarcomeric gene titin (*TTN*). The functional and physiological consequences of *RBM20* mutations outside the mutational hotspot of *RBM20* have not been explored to date. In this study, we investigated the pathomechanism of DCM caused by a novel *RBM20* mutation in human cardiomyocytes.

Methods and results We identified a family with DCM carrying a mutation ($RBM20^{E913K/+}$) in a glutamate-rich region of RBM20. Western blot analysis of endogenous RBM20 protein revealed strongly reduced protein levels in the heart of an $RBM20^{E913K/+}$ carrier. RNA deep-sequencing demonstrated massive inclusion of exons coding for the spring region of titin in the $RBM20^{E913K/+}$ carrier. Titin isoform analysis revealed a dramatic shift from the less compliant N2B towards the highly compliant N2BA isoforms in $RBM20^{E913K/+}$ heart. Moreover, an increased sarcomere resting-length was observed in single cardiomyocytes and isometric force measurements revealed an attenuated Frank–Starling mechanism (FSM), which was rescued by protein kinase A treatment.

Conclusion A mutation outside the mutational hotspot of *RBM20* results in haploinsufficiency of *RBM20*. This leads to disturbed alternative splicing of *TTN*, resulting in a dramatic shift to highly compliant titin isoforms and an impaired FSM. These effects may contribute to the early onset, and malignant course of DCM caused by *RBM20* mutations. Altogether, our results demonstrate that heterozygous loss of RBM20 suffices to profoundly impair myocyte biomechanics by its disturbance of *TTN* splicing.

Keywords Sarcomere • Cardiomyopathy • Dilated cardiomyopathy • Heart failure • Alternative splicing • RBM20

*Corresponding author. Tel: +31 20 5664678; fax: +31 20 6976177, E-mail: a.beqqali@icloud.com

1. Introduction

Dilated cardiomyopathy (DCM) is characterized by cardiac dilatation and systolic dysfunction, which is the leading cause of heart transplantation. In total, 25–50% of DCM cases are familial and causative mutations have been described in more than 50 genes encoding mostly structural components of cardiomyocytes.[1]

Recently, mutations in the RNA-binding motif protein 20 (RBM20) were shown to cause an early onset and clinically aggressive form of DCM.[2,3] Subsequently, next-generation sequencing (NGS) in a large cohort of idiopathic DCM (iDCM) patients revealed that *RBM20* belongs to the most frequently affected genes in DCM.[4]

Studies in rodents demonstrated that RBM20 expression is highly enriched in the heart and regulates the alternative splicing of a set of genes of which titin (*TTN*) is its most prominent target.[5–9]

Altered splicing of *TTN* occurs in a number of cardiac diseases, such as heart failure, ischaemic heart disease, and hypertrophic cardiomyopathy.[10] Studies have shown a shift in expression from the stiff N2B isoform of titin towards the compliant N2BA isoform in human cardiomyopathies. This shift has been associated with reduced myofibrillar stiffness in DCM patients,[11,12] which has been proposed to improve diastolic filling.[7,13] In addition, an increase in compliant titin has also been suggested to impair systolic performance by affecting the Frank–Starling mechanism (FSM), i.e. the ability of the sarcomere to increase contractile force in response to stretch.[13]

Rbm20 knock out rats showed altered splicing of *TTN* and developed cardiomyopathy, which provides additional evidence for its causal role in disease development. The functional and physiological consequences of human *RBM20* mutations at the cardiomyocyte and sarcomere level are unknown. Here, we show that a novel mutation outside the proposed mutational hotspot[2,3] leads to missplicing of *TTN* resulting in increased compliance of cardiomyocytes with subsequent Ca^{2+}-sensitized sarcomeres, and an impaired FSM in human cardiomyocytes. Treatment of *RBM20* mutant cardiomyocytes with the downstream kinase of the β-adrenergic receptor restored the FSM, whereas active and passive forces at submaximal, physiologic calcium concentrations were lower compared with controls. Our data indicate that heterozygous loss of RBM20 decreases its levels sufficiently to shift *TTN* splicing towards highly compliant isoforms and thereby lower force generated by sarcomeres.

2. Methods

2.1 Clinical and genetic investigations

All individuals underwent clinical examinations in a dedicated cardiomyopathy clinic at Aarhus University Hospital including 12-lead electrocardiogram, two-dimensional echocardiography, and a coronary angiogram if indicated. Diagnosis of familial DCM was based on diagnostic criteria.[14] The proband was included in the INHERITANCE (Integrated Heart Research In Translational Genetics of Cardiomyopathies in Europe) project after oral and written informed consent. The local ethics committee approved the study protocol (M-20110014).

2.2 Myocardial tissue

Myocardial biopsies of the proband's explanted heart were obtained immediately after removal from the patient and were snap-frozen in liquid nitrogen and stored at −80 °C or fixated in 4% paraformaldehyde until further processing.

Left ventricular (LV) samples from end-stage heart failure patients with idiopathic DCM were obtained during heart transplant surgery. Tissue from donor hearts served as reference for non-failing myocardium (controls). Samples were obtained after informed consent and with approval of the local Ethics Committee (St Vincent's Hospital Human Research Ethics Committee, Sydney, Australia: File number: H03/118; Title: Molecular analyses of human Heart Failure) and by The University of Sydney HREC number 12146. The investigation conforms to the principles outlined in the Declaration of Helsinki (1997).

2.3 Plasmid constructs

Full-length *Rbm20* cDNA with an N-terminal FLAG-tag was amplified by polymerase chain reaction (PCR) from mouse heart cDNA and cloned into pCRII-TOPO (Invitrogen, Carlsbad, CA, USA). Next, cDNA encoding Rbm20 with an N-terminal FLAG epitope was subcloned into the pcDNA3.1 (Invitrogen, Carlsbad, CA, USA) expression vector.

Mutagenesis was performed using the QuickChange II Site-directed mutagenesis kit (Agilent Technologies, Santa Clara, CA, USA) according to the manufacturer's instructions. All cloning products were confirmed by sequencing.

2.4 Cell culture and transient transfection

U2-OS cells were cultured in Dulbecco's modified Eagle's medium (Life technologies, Carlsbad, CA, USA) containing 10% foetal calf serum (Life technologies, Carlsbad, CA, USA).

For western blot analysis, cells were plated in six-well plates 1 day before transfection. For immunocytochemistry, cells were plated on glass coverslips in a 12-well plate 1 day before transfection. U2-OS cells were transiently transfected using Lipofectamin 2000 (Invitrogen, Carlsbad, CA, USA) according to the manufacturer's protocol and analysed 48 h after transfection.

2.5 Myocyte isolation and GapmeR transfection

Neonatal rat cardiomyocytes (NRCMs) were isolated as previously described.[15] NRCMs were plated on fibronectin-coated (Corning Life Science, Corning, NY, USA) six-well plates (750 000 cells/well). Cells were serum-starved for 24 h, after which they were transfected with GapmeRs (Exiqon, Vedbaek, Denmark final concentration 25 nM) against *Rbm20* (Rbm20-1: 5′-GTAATGATTGACGAG-3′ Rbm20-2: 5′-ACTTAGCTTTAGTCT-3′) or a negative control (300610) using Lipofectamine 2000 (Thermo Fisher Scientific, Waltham, MA, USA) according to manufacturer's protocol.

Cells were harvested 48 h after transfection and RNA was processed for reverse transcriptase (RT)–PCR and quantitative RT–PCR as described below.

2.6 Western blot

Western blotting was performed according to standard protocols. Briefly, protein concentrations were determined using the BCA protein assay (Pierce, Rockford, IL, USA) and proteins were resolved by SDS-PAGE and transferred to polyvindyline difluoride (PVDF) membrane (Bio-Rad, Hercules, CA, USA). PVDF membranes were incubated overnight at 4°C with the following primary antibodies: rabbit anti-FLAG (1:1000; Thermo scientific, Waltham, MA, USA), mouse anti-glyceraldehyde phosphate dehydrogenase (GAPDH) (1:5000; Fitzgerald Industries International, Acton, MA, USA). Horseradish peroxidase-conjugated secondary antibodies (Amersham Biosciences, Little Chalfont, UK) were used for detection and were incubated for 1 h at room temperature (RT). Western blots were developed with ECL prime Western blotting detection reagent

(Amersham Biosciences, Little Chalfont, UK) and images were acquired using the ImageQuant LAS4000 (GE Healthcare Europe, Eindhoven, The Netherlands). Densitometric analysis of Western blots was performed using Image J software.

2.7 Quantitative real time PCR

RNA was isolated from tissue or cells using TRIzol (Invitrogen, Carlsbad, CA, USA) according to the manufacturer's protocol. Subsequently, 1 µg RNA was treated with DNAse I (Invitrogen, Carlsbad, CA, USA) and cDNA was synthesized using Superscript II RT (Invitrogen, Carlsbad, CA, USA). Quantitative PCR (qPCR) was performed on a Lightcycler 480 (Roche Diagnostics, Risch-Rotkreuz, Switzerland) using SYBR green (Roche Diagnostics, Risch-Rotkreuz, Switzerland). Gene expression was normalized to *Gapdh* expression. Analysis of qPCR data was performed using LinRegPCR analysis software.[16]

2.8 Immunocytochemistry

Cells were fixed in 2% paraformaldehyde for 30 min, washed three times in phosphate buffered saline (PBS), and permeabilized in 0.1%Triton-X/PBS for 8 min. Cells were blocked in 4% normal goat serum (NGS) for 1 h at RT and then incubated with first antibody in 4% NGS overnight at 4°C. Secondary antibody incubation occurred in 4% NGS for 1 h at RT. Nuclear staining was performed as a last step using DAPI (Molecular Probes, Eugene, OR, USA). Coverslips were then mounted on glass slides with Mowiol (Calbiochem, San Diego, CA, USA) and images were captured using confocal microscopy (Leica SP8, Leica Microsystems, Wetzlar, Germany). Primary antibodies were as follows: rabbit anti-FLAG (1:200; Thermo Scientific, Waltham, MA, USA). Alexa Fluor® 488 conjugated secondary antibody was used at 1:250 (Invitrogen, Carlsbad, CA, USA).

2.9 Immunohistochemistry

Human LV biopsies were fixed in 4% paraformaldehyde overnight and embedded in paraffin. Antigen retrieval was performed by microwave heating of tissue sections (7 µm) in citrate buffer (pH 6) after which primary antibody incubation occurred overnight at 4°C. The following primary antibodies were used: custom made rabbit anti-RBM20 (1:100; Eurogentec, Liège, Belgium) and mouse anti-alpha actinin (1:800; Sigma-Aldrich, Zwijndrecht, The Netherlands). Alexa Fluor® 488 and Alexa Fluor® 568 conjugated secondary antibodies were used at 1:250 (Invitrogen, Carlsbad, CA, USA). Nuclear staining was performed as a last step using DAPI (Molecular Probes, Eugene, OR, USA) and images were captured using confocal microscopy (Leica SP8, Leica Microsystems, Wetzlar, Germany).

2.10 RNA sequencing and splicing analyses

Total RNA was isolated with TRIzol (Life Technologies, Carlsbad, CA, USA) according to manufacturer's instructions. RNA integrity was verified with the Agilent Bioanalyzer (Agilent Technologies, Santa Clara, CA, USA) before RNA sequencing (RNA-seq) libraries were prepared with the TruSeq RNA sample Preparation Kit (Illumina, San Diego, USA). RNA-seq on a HiSeq 2000 instrument (Illumina, San Diego, USA) and analysis were performed as described before.[5,6]

2.11 Reverse transcriptase-polymerase chain reaction

Total RNA was isolated from cells using Trizol reagent (Invitrogen, Carlsbad, CA, USA) according to standard protocol. DNAseI digestion was performed to ensure elimination of genomic DNA. Total RNA (1 µg) was transcribed by RT (SuperScript™ II RT, Invitrogen, Carlsbad, CA, USA) and used for PCR using HOT FIREPol DNA polymerase (Solis Biodyne, Tartu, Estonia). For each PCR reaction, 1 µL cDNA was used in a reaction volume of 50 µL. The cycling parameters were 95°C for 15 s; 58°C, 30 s; and 72°C, 45 s, for 30 cycles. The PCR cycles were preceded by an initial denaturation of 15 min at 95°C and followed by a final extension of 7 min at 72°C. Glyceraldehyde phosphate dehydrogenase (*Gapdh*) was used as RNA input control. As a negative control total RNA (-RT control), and a water sample were used directly for PCR.

2.12 Protein isoform analysis

Titin isoforms were separated on 1% agarose gel and stained with SYPRO Ruby protein stain as described previously[17] and measured in triplo. Titin size was estimated as previously described[17,18] by comparison of the relative mobility to myosin heavy chain (MHC) of adult mouse soleus, human control LV tissue, and DCM RBM20 mutant and was measured in triplo. Titin isoform ratio of RBM20 E913K was compared with iDCM samples (iDCM; $N = 4$) and control hearts ($N = 3$). All values indicated for titin isoform ratio and titin N2BA size are mean of triplo measurements.

2.13 Membrane-permeabilized cardiomyocyte measurements

Maximal and passive force of sarcomeres was measured in single membrane-permeabilized cardiomyocytes mechanically isolated from heart tissue as previously described.[19] Length-dependent activation and protein kinase A (PKA) incubations were performed as previously described.[20] Data are shown as mean ± S.E.M. N is the number of patients and n is the number of cardiomyocytes.

2.14 Statistical analysis

Statistical analyses were performed using Graph Pad Prism (GraphPad Software Inc., La Jolla, USA), SPSS (IBM Statistics, Armonk, NY, USA), and Excel (Microsoft corporation, Albuquerque, NM, USA).

Data sets that follow a normal distribution were statistically compared with unpaired *t*-test, e.g. Western blot quantifications (*Figure 2A* and *C*) and nuclear/cytoplasmic ratio quantifications in Supplementary material online, *Figure S1*.

A one-way analysis of variance (ANOVA) was used to compare resting sarcomere lengths of cardiomyocytes of control ($N = 3$, $n = 32$), iDCM ($N = 3$, $n = 49$), and E913K RBM20 ($N = 1$, $n = 45$) cardiomyocytes after normal distribution was confirmed by Kolmogorov–Smirnov test.

For passive force measurements, normal distribution was confirmed by Kolmogorov–Smirnov test after which a one-way ANOVA with Holm–Sidak *post hoc* test was used to compare means between groups.

The means of calcium sensitivity were compared with the non-parametric Kruskal–Wallis with Dunn's *post hoc* test.

For statistically significant differences the *P*-value is noted, for differences that were not statistically significant (N.S.) is noted in figure legends. Raw data are available in as Supplementary material online, Supplementary data file S1.

A *P*-value of <0.05 was considered significant. All data are expressed as mean ± S.E.M. The significance level was indicated as follows: $*P < 0.05$; $**P < 0.01$; $***P < 0.001$.

An expanded Methods section is available in the Supplementary mate rial online.

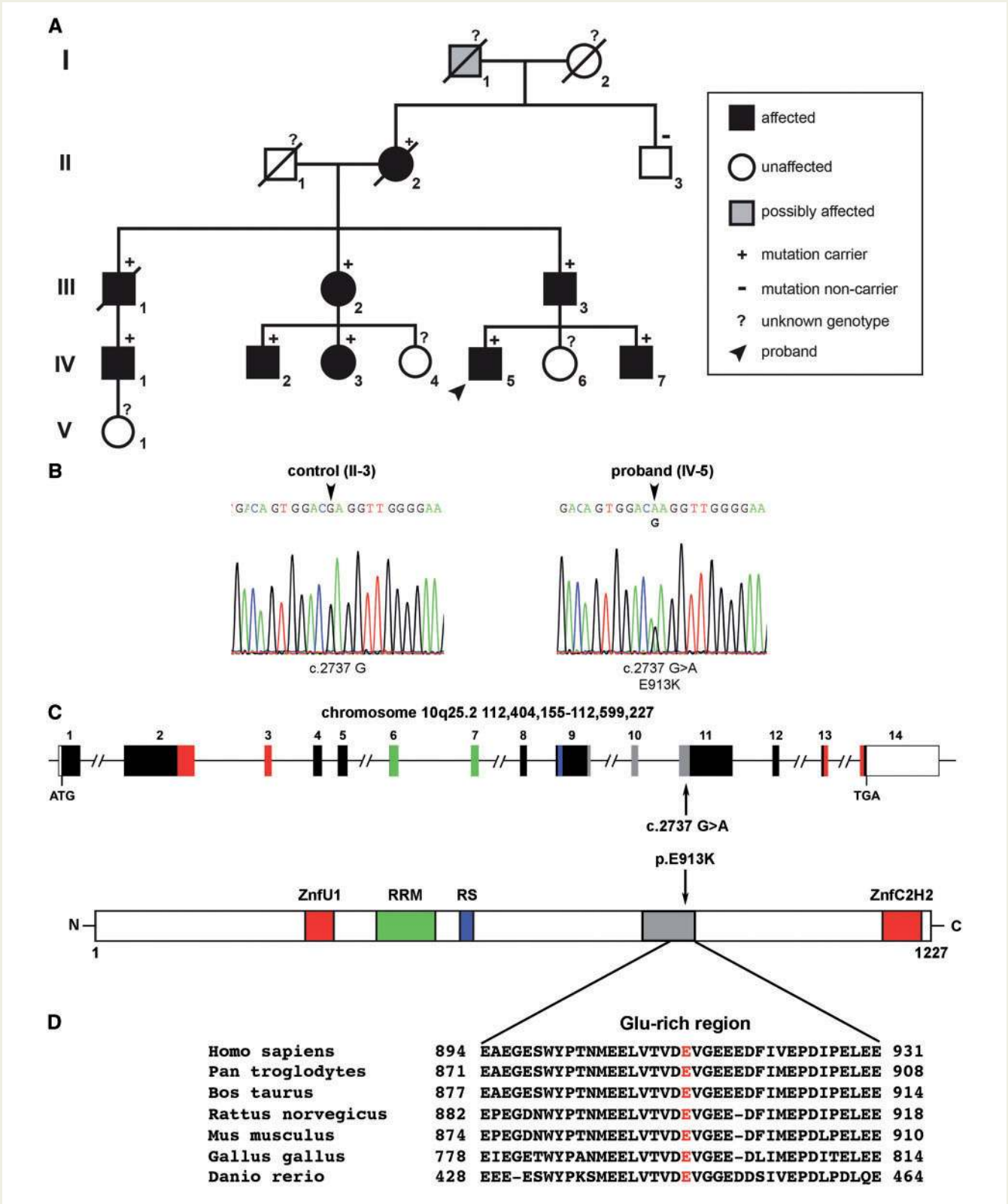

Figure 1 Identification of a novel *RBM20* mutation in a family with DCM. (*A*) Family carrying an *RBM20* c.2737 G>A variant. (*B*) Confirmation of the variant by Sanger sequencing. (*C*) Genomic organization of the human *RBM20* gene and schematic representation of RBM20 protein with predicted functional domains: Zinc finger U1 and Zinc finger C2H2 type (red), RNA-Recognition motif (green), and arginine/serine-rich domain (RS) in blue. (*D*) Amino acid alignment of RBM20 glutamate-rich domain with mutated residue in red.

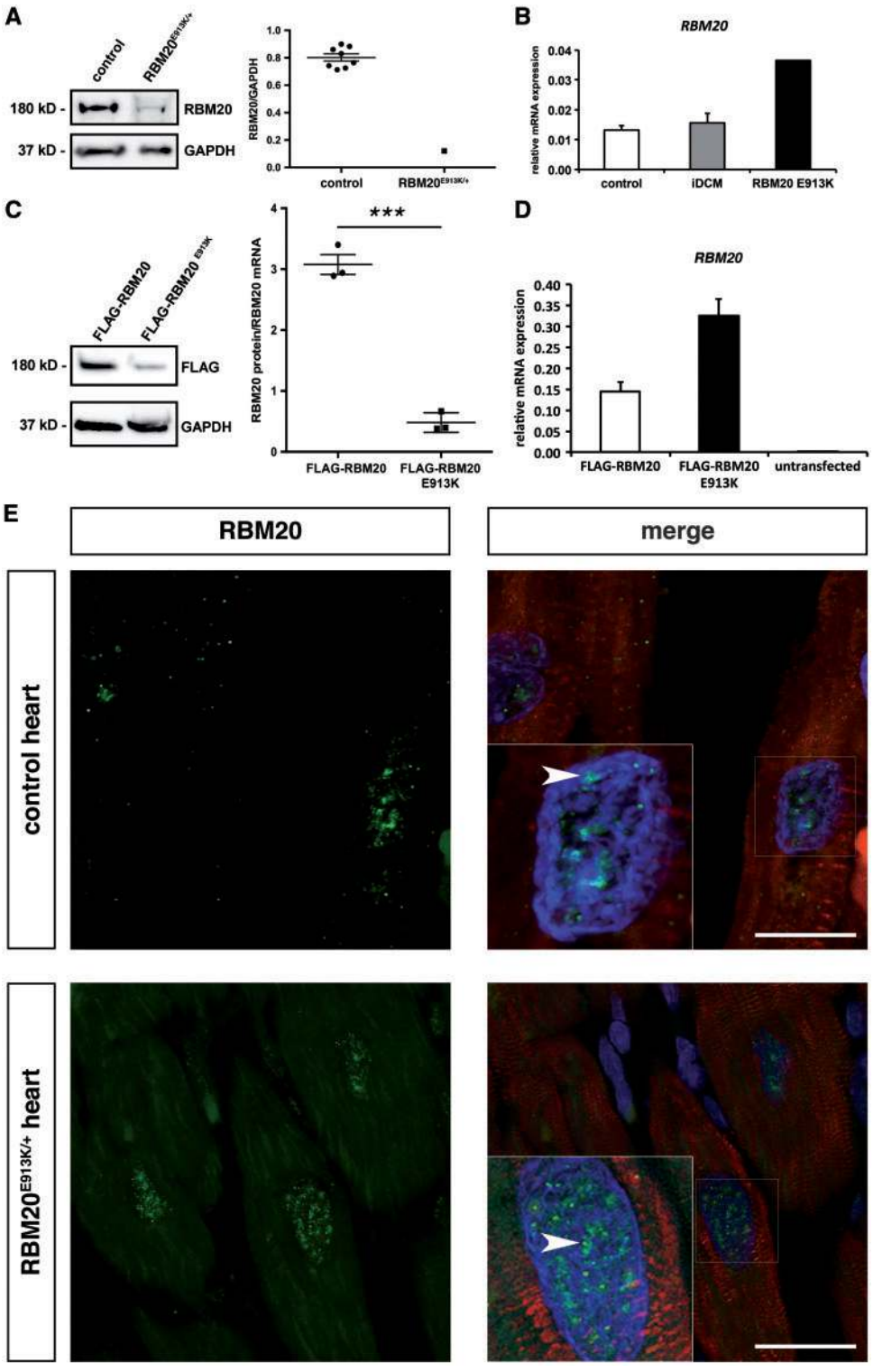

Figure 2 E913K mutation leads to lower RBM20 protein levels. (*A*) Immunoblot for endogenous RBM20 in control and RBM20$^{E913K/+}$ heart with quantification of Western blot (right panel, control $N = 8$, RBM20$^{E913K/+}$ $N = 1$ in triplicate). (*B*) qPCR analysis of *RBM20* mRNA in control ($N = 5$), iDCM ($N = 3$) and RBM20$^{E913K/+}$ ($N = 1$) LV tissue. (*C*) Immunoblot of U2-OS cells transfected with FLAG-RBM20 and FLAG-RBM20^{E913K}. GAPDH was used as loading control. Quantification of immunoblot for FLAG-RBM20 and mutant as determined by densitometry and normalized for *RBM20* mRNA (values represent the averages from three independent experiments); *t*-test ***$P < 0.001$. (*D*) qPCR analysis of *RBM20* mRNA in transfected U2-OS cells ($N = 3$ independent experiments). (*E*) Subcellular localization of endogenous RBM20 in control and RBM20$^{E913K/+}$ heart (green). White arrows indicate the nuclear localization of RBM20 aggregates. Cardiomyocytes were stained for alpha-actinin (red) and nuclei were stained with DAPI (blue). Scalebar: 10 μm.

3. Results

3.1 Identification of a novel *RBM20* variant in a family with DCM

From a recently published screen in a European cohort of 639 iDCM patients,[4] we identified a novel heterozygous variant in *RBM20* (NM_001134363.1 c.2737G > A). Genetic analyses of the pedigree showed that the variant co-segregated with DCM and transmitted as an autosomal dominant trait with complete penetrance (*Figure 1A*). The NGS results were confirmed with Sanger sequencing (*Figure 1B*). No other mutations were identified in 83 DCM genes, including *TTN*.[4] The variant was absent in more than 60 000 exomes [Exome Aggregation Consortium (ExAC), Cambridge, MA, URL: http://exac.broadinstitute.org, January 2015]; however, it is annotated in the dbSNP database (http://www.ncbi.nlm.nih.gov/SNP/index.html) as a variant of uncertain significance (rs397516607) with no frequency data available.

The index patient (III-3) presented with decompensated heart failure at the age of 35. An echocardiogram showed an LVEF of 10% and a restrictive LV filling pattern in absence of coronary atherosclerosis. Endomyocardial biopsies were consistent with DCM and demonstrated hypertrophy and fibrosis without signs of myocarditis. Medical heart failure therapy was initiated following a recovery of systolic function to a stable LVEF of 45% 11 years after initial diagnosis. The brother (III-1) and the mother (II-2) both died of heart failure at the ages of 29 and 72, respectively. Evaluation of remaining family members identified six individuals with clinical signs of DCM, including the proband (IV-5) who despite medical therapy developed terminal heart failure and required heart transplantation (*Figure 1A*). Other family members were less affected and had only mild impairment of LVEF. Detailed clinical characteristics of the proband and relatives are shown in Supplementary mate rial online, *Table S1*.

The identified variant is located in exon 11, and leads to an amino acid change at position 913 from a negatively charged and acidic glutamate to a positively charged and basic lysine residue (*Figure 1C*). We examined the putative functional effect of the p.E913K mutation by using the prediction algorithms Polyphen-2 and SIFT (Sorting intolerant from tolerant)[21,22] which predicted this amino acid change to be 'probably damaging' (HVAR (Human variation) score 0.994) and 'deleterious' (SIFT score: 0), respectively.

When aligning the amino acid sequence of RBM20 in different species, we observed that the affected glutamate residue lies within an evolutionary highly conserved glutamate-rich (34%) region, which likely represents a domain of functional importance (*Figure 1D*).

3.2 E913K mutation decreases stability of the RBM20 protein

To assess whether the *RBM20* mutation acts as dominant-negative or leads to haploinsufficiency, we investigated endogenous RBM20 protein levels in cardiac tissue of subject IV-5 who underwent heart transplantation at 19 years of age.

Western blot analysis showed a strong downregulation of RBM20 protein levels in the patient as compared with the control hearts (*Figure 2A*).

Quantitative PCR analysis demonstrated that *RBM20* mRNA levels were not down-regulated in the RBM20 patient as compared with healthy controls and iDCM samples suggesting that the mRNA stability is not affected by the c.2737G > A variant (*Figure 2B*).

To further investigate whether the E913K mutation has an effect on RBM20 protein stability, we generated a FLAG-tagged construct of the mutant RBM20 and transfected it in U-2 OS cells. Western blot analysis showed a lower RBM20 protein level for the E913K mutant compared with wildtype RBM20 (*Figure 2C*). qPCR on the transfected cells revealed no sign of *RBM20* mRNA degradation, which rules out that the observed decrease in RBM20 protein is due to differences in transfection efficiency (*Figure 2D*). Densitometric analysis revealed an 80% lower RBM20 protein to *RBM20* mRNA ratio in the E913K mutant-transfected cells (*Figure 2C*).

We did not observe an effect of the E913K mutation on the subcellular localization of RBM20 in histological sections of the RBM20$^{E913K/+}$ heart (*Figure 2E*; mutant RBM20 fluorescent signal was digitally enhanced for better visualization). RBM20 was located predominantly in sub-nuclear foci of cardiomyocytes, as evidenced by co-staining with the cardiomyocyte marker alpha-actinin. The weak fluorescent signal for RBM20 in the RBM20$^{E913K/+}$ hearts supported our findings of RBM20 haploinsufficiency.

Furthermore, we investigated subcellular distribution of wildtype and mutant RBM20 in the easy to transfect cell line U-2 OS. Although RBM20 has been described as exclusively nuclear, we also observed cytoplasmic localization in these cells (see Supplementary material online, *Figure S1A*; fluorescent signal of RBM20-E913K was digitally enhanced for better visualization). To assess whether the mutant RBM20 has influence on the nucleus to cytoplasm ratio of RBM20, we quantified subcellular immunofluorescence and found no significant changes between the wildtype and RBM20-E913K-transfected cells (see Supplementary material online, *Figure S1B*). Together, these findings suggest that RBM20$^{E913K/+}$ drives pathogenesis through a mechanism mediated by haploinsufficiency.

3.3 RBM20$^{E913K/+}$ mutation affects *TTN* splicing

To determine whether RBM20$^{E913K/+}$ affects *TTN* splicing, we performed RNA-seq on LV tissue of subject IV-5. Splicing analysis revealed that long stretches of exons in *TTN* were misspliced in RBM20$^{E913K/+}$ LV compared with a control subject and a non-RBM20 DCM patient. In particular, a higher percentage (expressed as 'Percentage Spliced In') of the exons encoding the elastic PEVK (PSI 85–95% in RBM20$^{E913K/+}$ vs. 70–80% in control) and immunoglobulin-rich region (PSI 60–90% in RBM20$^{E913K/+}$ vs. 5–80% in control) was included in the titin transcripts of the RBM20$^{E913K/+}$ patient (*Figure 3A*).

We confirmed the inclusion of exons in *TTN* by RT–PCR in a region that encodes part of the PEVK region that was shown to be subject to RBM20-dependent splicing.[5] In myocardial samples of iDCM hearts, splicing of *TTN* in this region appeared similar to control hearts (*Figure 3B*). In addition, we confirmed the increase in exon inclusion in the middle Ig region of titin by qPCR (see Supplementary material online, *Figure S2A*). Interestingly, the RNA-seq results showed regions of exon inclusion in the RBM20$^{E913K/+}$ heart, which we confirmed with qPCR (see Supplementary material online, *Figure S2B*).

To assess whether the differential splicing pattern of *TTN* is indeed a result of reduced RBM20 levels, we performed Rbm20 knockdown experiments in NRCMs. Splicing of the PEVK region of rat *titin* was similar to that of the RBM20$^{E913K/+}$ patient, as shown by splice RT–PCR (*Figure 3C*).

To determine whether these splicing changes are also reflected in the titin protein, we investigated titin isoforms by SDS-agarose gel

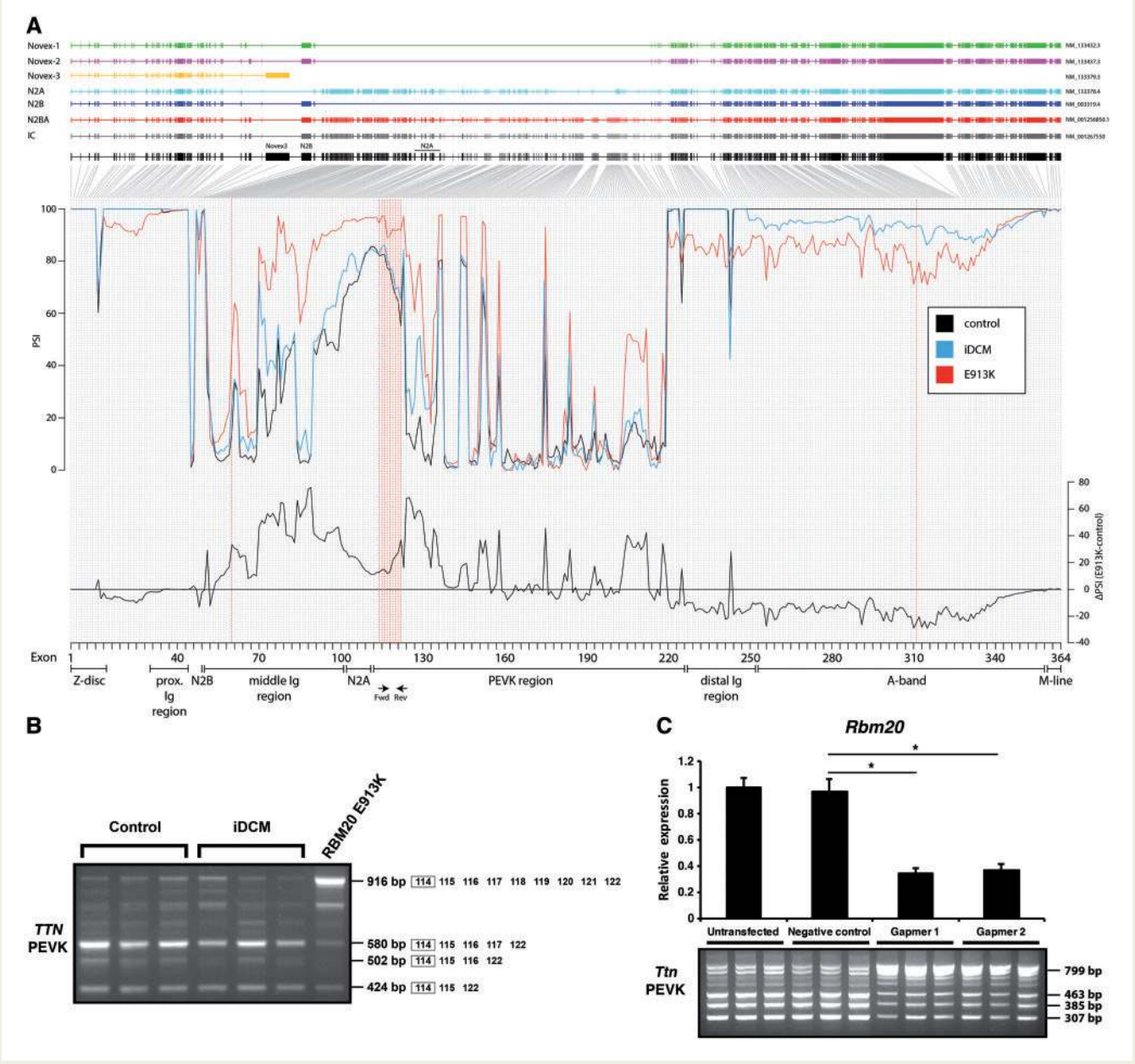

Figure 3 RBM20$^{E913K/+}$ affects *titin* mRNA splicing. (*A*) Percentage Spliced In (PSI) plot of titin mRNA as determined by RNA-seq on control ($N = 1$), iDCM ($N = 1$), and RBM20$^{E913K/+}$ ($N = 1$) heart. Titin isoforms are indicated in different colours. Exons that are validated by PCR are indicated with red dashed lines. (*B*) RT–PCR of titin PEVK region spanning exons 114–22 on control ($N = 3$), iDCM ($N = 3$), and RBM20$^{E913K/+}$ heart ($N = 1$). (*C*) Upper panel: qPCR for *Rbm20* in NRCMs transfected with GapmeRs to induce *Rbm20* knockdown. Lower panel: Splice-RT–PCR of titin PEVK region in Rbm20 knockdown cardiomyocytes vs. control GapmeRs and untransfected cardiomyocytes.

electrophoresis. Titin isoforms in the RBM20$^{E913K/+}$ patient showed a dramatic shift towards more compliant titin isoforms evident from a higher N2BA/N2B ratio (7.45) compared with 0.54 ± 0.04 and 0.96 ± 0.27 in control and iDCM hearts, respectively (*Figure 4A*).

Also, a wider N2BA band was visible (*Figure 4A*) compared both with donor and iDCM samples, indicating alternative N2BA products at protein level. Therefore, the mobility of the compliant titin of the RBM20$^{E913K/+}$ sample was compared with that of samples with various proteins of known size (nebulin and N2A of an adult mouse soleus muscle and N2B of a human non-failing control left ventricle) during simultaneous gel electrophoresis. We constructed a reference line of molecular weight in relation to the mobility relative to MHC. Titin size estimation showed titin products in the RBM20$^{E913K/+}$ LV of 2849 kDa (N2B) and a predominant 3390–3921 kDa (N2BA) isoform (*Figure 4B*). This is a larger so-called giant N2BA (N2BA-G) compared with the conventional N2BA isoform of ~3300 kDa.[23] These findings suggest that the RBM20$^{E913K/+}$ mutation strongly alters *TTN* splicing and protein isoform composition leading to an increase in larger and more compliant titin isoforms.

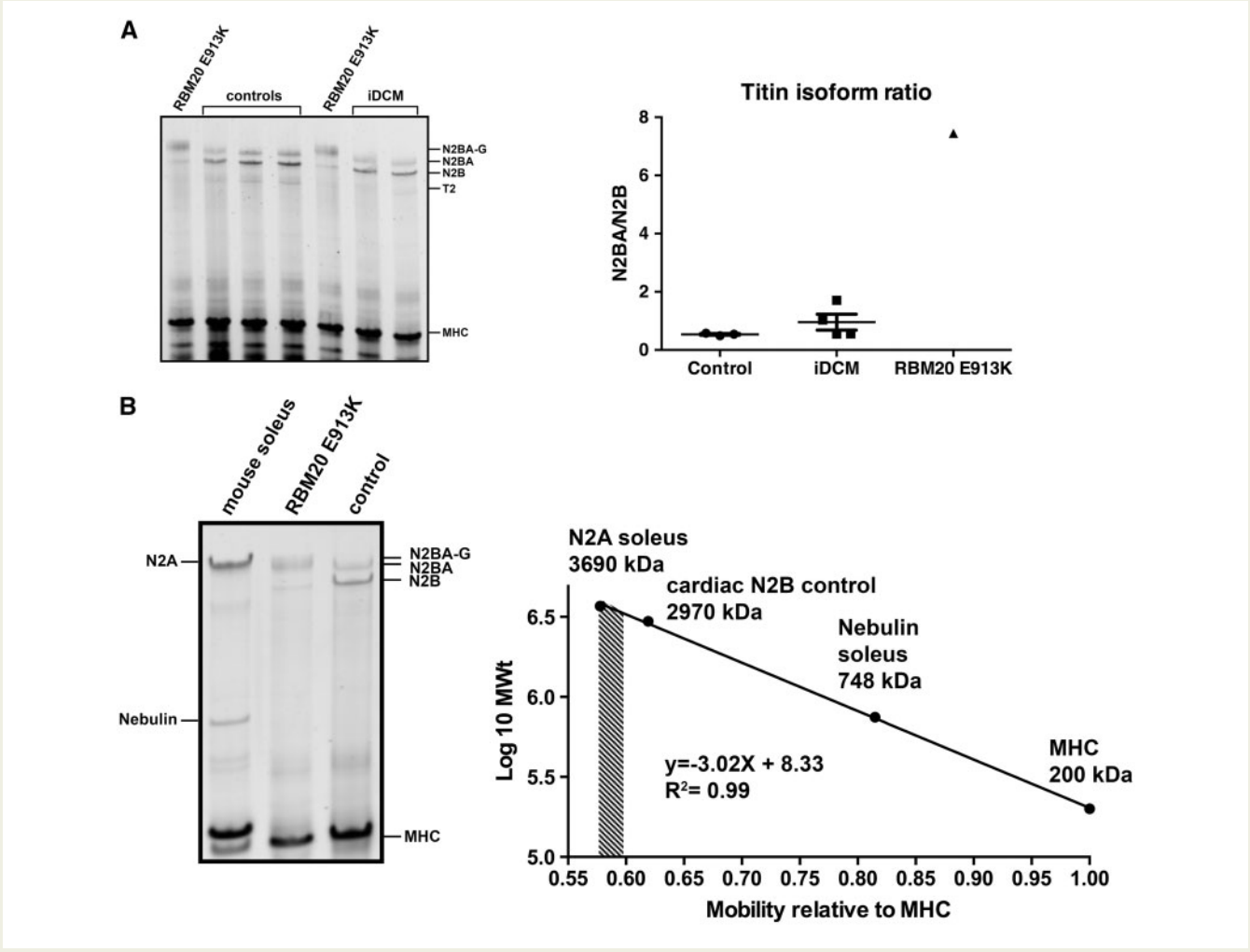

Figure 4 RBM20$^{E913K/+}$ results in larger *titin* protein isoforms production. (*A*) Representative SDS-agarose gel of titin isoforms in controls, iDCM, and RBM20$^{E913K/+}$ patient. Right panel: Quantification of N2BA/N2B ratio as determined by densitometry analysis in controls ($N = 3$), iDCM ($N = 4$), and RBM20$^{E913K/+}$ patient ($N = 1$). Values shown are mean of triplo measurements. (*B*) Molecular weight estimation of titin isoforms in RBM20$^{E913K/+}$ patient as determined by relative mobility assay.

3.4 The Frank–Starling mechanism is impaired in RBM20$^{E913K/+}$ cardiomyocytes

We hypothesized that the RBM20$^{E913K/+}$-induced shift towards more compliant titin affects cardiomyocyte stiffness. Correspondingly, a significantly higher resting sarcomere length ($P < 0.0001$) of the RBM20$^{E913K/+}$ cardiomyocytes was observed after cell isolation compared with both control and iDCM (*Figure 5A*). In addition, due to the highly compliant N2BA-G cardiomyocytes could easily be stretched to a sarcomere length of 2.4 μm and measure isometric force in the RBM20$^{E913K/+}$ cardiomyocytes (*Figure 5B*). Functional measurements of maximal force at saturating calcium concentrations showed no difference between RBM20$^{E913K/+}$ compared with control hearts (data not shown). Passive stiffness measured over a range of sarcomere lengths, revealed a similar passive force development in RBM20$^{E913K/+}$ cardiomyocytes at shorter sarcomere lengths whereas a trend towards a decreased passive tension in RBM20$^{E913K/+}$ cardiomyocytes at the higher sarcomere lengths 2.3 and 2.4 μm was observed (N.S.) compared with both control and iDCM hearts (*Figure 5C*).

As changes in titin isoform composition may alter the FSM,[13] we measured force development at various [Ca^{2+}] and increasing sarcomere lengths. RBM20$^{E913K/+}$ cardiomyocytes showed increased myofilament Ca^{2+}-sensitivity and decreased slope compared with control cardiomyocytes at a sarcomere length of 2.2 μm (see Supplementary material online, *Figure S3*). The Ca^{2+}-sensitivity is expressed as EC_{50}, defined as the [Ca^{2+}] needed to achieve 50% of maximal force development. The RBM20$^{E913K/+}$ cardiomyocytes showed higher Ca^{2+}-sensitivity at all sarcomere lengths compared with control hearts and a blunted FSM (*Figure 5D*), evident from a smaller length-dependent increase in Ca^{2+}-sensitivity ($\Delta EC_{50} = 0.83 \pm 0.27$ and 0.30 ± 0.04 in control and RBM20$^{E913K/+}$, respectively; *Figure 5D*).

Myofilament Ca^{2+}-sensitivity was also higher (*Figure 5D*) and FSM smaller ($\Delta EC_{50} = 0.49 \pm 0.14$) in iDCM compared with control cells. This indicates that a common protein modification, such as lower protein phosphorylation, underlies the differences in myofilament functional properties between DCM and control samples. PKA-mediated sarcomere protein phosphorylation in length-

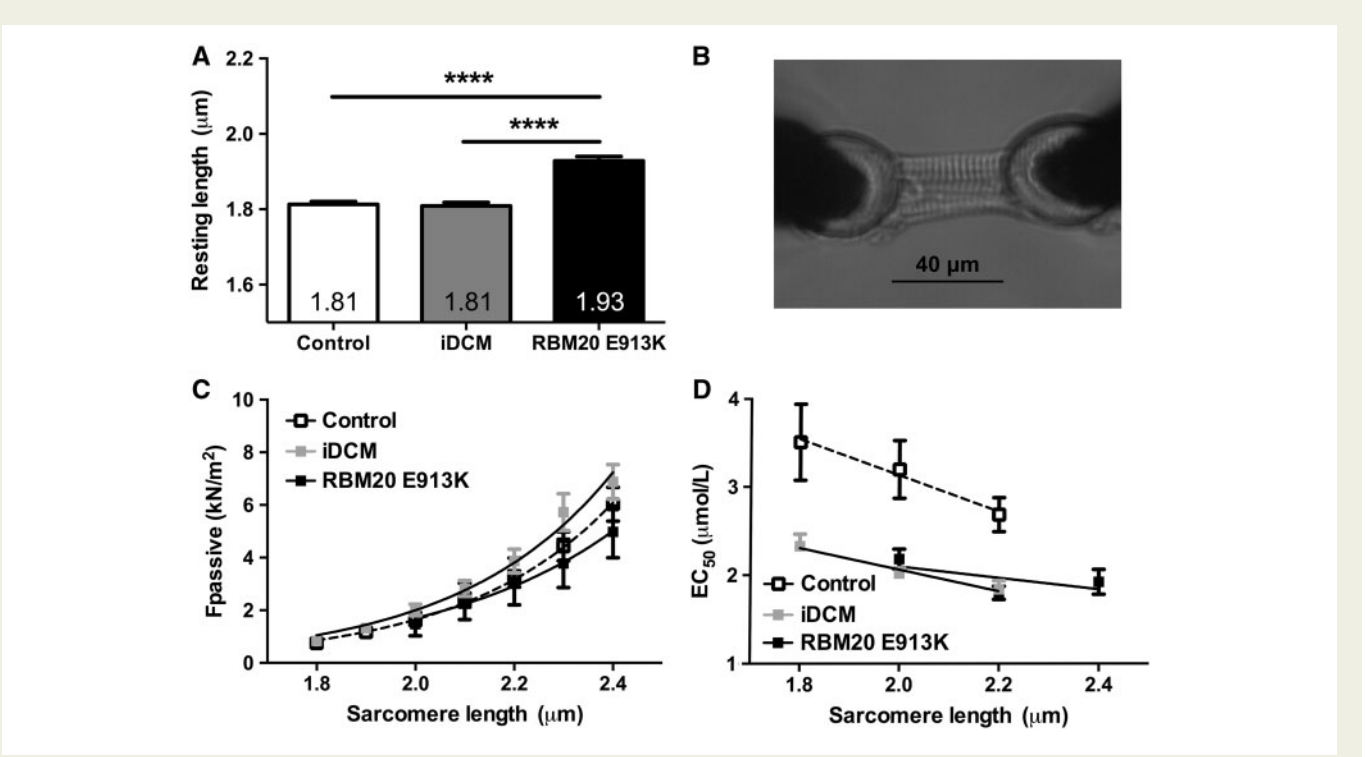

Figure 5 Sarcomere length is increased in RBM20$^{E913K/+}$ cardiomyocytes. (*A*) Slack sarcomere length of RBM20$^{E913K/+}$ ($N = 1$, $n = 45$) cardiomyocytes was significantly higher compared with control ($N = 3$, $n = 32$) and iDCM ($N = 3$, $n = 49$) cardiomyocytes (****$P < 0.0001$). (*B*) RBM20$^{E913K/+}$ cardiomyocyte at a sarcomere length of 2.4 μm. (*C*) Passive force in cardiomyocytes of control ($N = 3$, $n = 16$), iDCM ($N = 3$, $n = 19$), and RBM20$^{E913K/+}$ ($N = 1$, $n = 6$) at different sarcomere lengths as determined by isometric force measurements was not different (N.S.) between groups. (*D*) Length-dependent activation in iDCM ($N = 3$, $n = 10$) and RBM20$^{E913K/+}$ ($N = 1$, $n = 9$) compared with control ($N = 2$, $n = 4$) cardiomyocytes.

dependent sarcomere activation enhances the length-dependent shift in the force-Ca^{2+} relation.[24]

To test whether high Ca^{2+}-sensitivity and the blunted length-dependent myofilament activation could be corrected by PKA-mediated phosphorylation, force measurements were performed after treatment with exogenous PKA. PKA treatment unmasked lower passive force development in RBM20$^{E913K/+}$ compared with both controls and iDCMs (*Figure 6A*). EC_{50} increased over the entire range of sarcomere lengths in RBM20$^{E913K/+}$ to levels above control and iDCM hearts (*Figure 6A* and *C*), indicating lower myofilament Ca^{2+}-sensitivity in RBM20$^{E913K/+}$ after PKA treatment. Higher EC_{50} indicates a lower Ca^{2+}-sensitivity of myofilaments in RBM20$^{E913K/+}$ compared with controls and iDCMs after PKA treatment (*Figure 6D*). Moreover, after PKA the slope of Ca^{2+}-sensitivity values at various sarcomere lengths of RBM20$^{E913K/+}$ increased in a manner similar to that observed in controls indicating restoration of the FSM (*Figure 6B*).

4. Discussion

Mutations in *RBM20* have recently been identified to segregate with DCM in humans and loss of RBM20 in rats induces altered splicing of titin.[2,3,5] Here, we demonstrated that a novel mutation in *RBM20* in a yet uncharacterized glutamate-rich domain decreased the stability of RBM20 protein and resulted in an abnormal inclusion of exons coding for the extensible I-band region of titin. This led to a massive shift from the N2B to highly compliant N2BA-titin isoforms. RBM20$^{E913K/+}$ cardiomyocytes had decreased length-dependent activation, which was rescued by PKA treatment. Moreover, PKA-mediated protein phosphorylation revealed lower passive force development and decreased calcium sensitivity at physiological [Ca^{2+}] in RBM20$^{E913K/+}$ cardiomyocytes compared with control and iDCM cardiomyocytes over a range of sarcomere lengths. A limitation in our study was the availability of human cardiac tissue of only one patient. Although this was the case, we believe our data shed new light on the molecular mechanism involved in *RBM20*-related DCM in human cardiomyocytes.

The c.2737G > A mutation is located in exon 11 of the *RBM20* gene, outside the previously described hotspot in exon 9, and alters an amino acid in an evolutionary conserved glutamate-rich region. Recent NGS studies described probands harbouring potential causal missense variants outside the RS-domain of RBM20.[4,25] Although mutations in *RBM20* are known to segregate with DCM, their effect on protein stability and function remains elusive. It is unknown whether these mutations act via dominant negative or rather via haploinsufficiency mechanisms. We showed that the E913K mutation strongly decreases endogenous and exogenous RBM20 protein levels without affecting its subcellular localization. This mutation could possibly lead to protein misfolding followed by proteasomal degradation. Interestingly, we observed a reduction of more than 50% of RBM20 protein levels in the RBM20$^{E913K/+}$ patient. This indicates that there might be a secondary mechanism that also influences the levels of the wildtype RBM20 protein. Although our findings strongly indicate a haploinsufficiency-mediated mechanism of disease, a dominant negative scenario cannot be excluded and would require mutation-specific antibodies or mass spectrometry approaches to discriminate between the wildtype and RBM20 mutant protein.

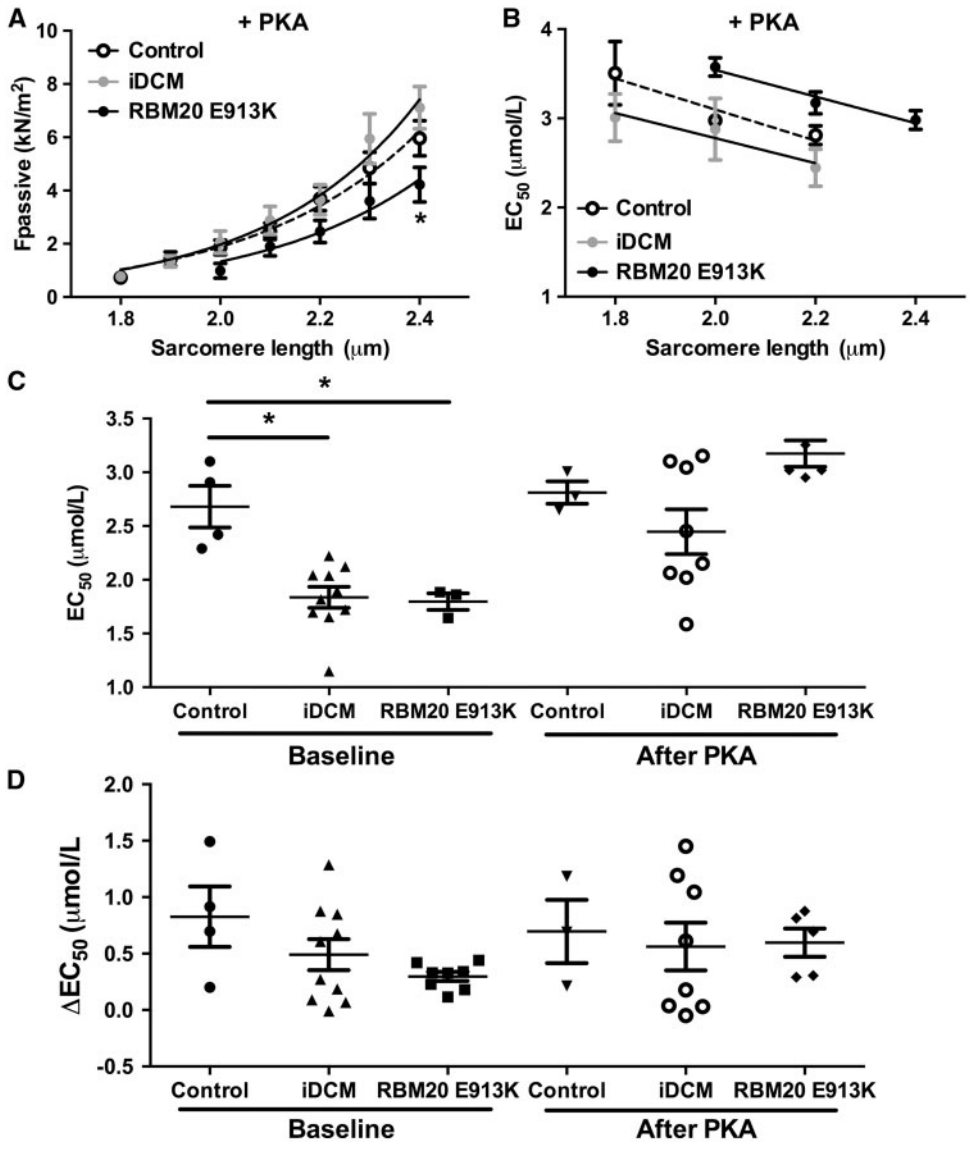

Figure 6 The Frank–Starling mechanism is impaired in RBM20$^{E913K/+}$ cardiomyocytes. (*A*) PKA treatment unmasked decreased passive force (statistically significant at sarcomere length 2.4 μm in RBM20^{E913K} compared with iDCM, *$P = 0.0373$) in cardiomyocytes of RBM20$^{E913K/+}$ ($N = 1$, $n = 6$) compared with control ($N = 3$, $n = 14$) and iDCM ($N = 3$, $n = 16$) cardiomyocytes at different sarcomere lengths. (*B*) Length-dependent activation in iDCM ($N = 2$, $n = 8$) and RBM20$^{E913K/+}$ ($N = 1$, $n = 5$) cardiomyocytes was rescued after PKA treatment to control ($N = 1$, $n = 3$) levels. (*C*) Calcium sensitivity at baseline was significantly increased in RBM20$^{E913K/+}$ (*$P = 0.0324$) and iDCM (*$P = 0.0201$) compared with control at a sarcomere length of 2.2 μm. Calcium sensitivity was decreased (N.S.) in RBM20$^{E913K/+}$ compared with iDCM and control after PKA treatment at a sarcomere length of 2.2 μm. (*D*) Length-dependent activation before and after PKA treatment.

In rats, RBM20 regulates titin splicing by acting as a splicing repressor on exons coding for the middle Ig region and PEVK domain in the extensible I-band region of titin.[26] Here, we demonstrated that repression of these exons is greatly reduced in the LV of an RBM20$^{E913K/+}$ patient, leading to erroneous inclusion of many exons in the mRNA of *titin*. Interestingly, *titin* splicing observed in the E913K patient is different from a previously reported mutation (S635A) in the RS-domain of RBM20, which results in *titin* exon inclusion only.[5] As the RS-domain is predicted to be involved in protein–protein interaction,[27] this mutation may affect the ability of RBM20 to interact with other spliceosome proteins, thus disrupting the normal RNA splicing process. However, RBM20$^{E913K/+}$ induces haploinsufficiency, resulting in both titin exon inclusion and exclusion, suggesting an additional role for RBM20 as a splice enhancer. Importantly, the RBM20 DCM patient did not carry a rare variant in *TTN* and 83 other DCM-related genes that could explain the aberrant alternative splicing in *TTN*. Overall, our results indicate that the amount of available wildtype RBM20 protein is critical to ensure proper splicing of titin.

The disturbed alternative splicing of titin in the RBM20$^{E913K/+}$ patient was reflected by the dramatic increase in titin N2BA/N2B isoform ratio. Previous studies showed that this ratio in healthy controls ranged from 0.4 to 0.8 whereas in iDCM and HF it ranged between 0.5 and 1.7.[11,12,28]

Here, we confirmed these ratios in the healthy donor and iDCM group. Strikingly, the RBM20$^{E913K/+}$ patient had an N2BA/N2B ratio of 7.45.

The much higher level of the N2BA giant isoforms of titins could explain the observed increase in slack sarcomere length in the RBM20$^{E913K/+}$ cardiomyocytes. An increase in slack sarcomere length was also found in a very recent study by Wyles *et al.*[29,30] using human-induced puripotent stem cell-derived cardiomyocytes from an RBM20$^{R636S/+}$ DCM patient. This highlights the importance of RBM20 in determining the N2BA/N2B ratio in the heart.

An increased N2BA/N2B ratio in disease was shown to correlate with a decreased passive stiffness of cardiomyocytes.[11,12] Although the N2BA/N2B ratio was much higher than previously reported for other types of heart disease, this did not translate to a proportional decrease of passive stiffness at short sarcomere lengths. Only at sarcomere lengths 2.3 and 2.4 µm a trend towards decreased passive force was observed. A possible explanation for this discrepancy could be that passive stiffness is determined not only by the ratio of compliant vs. stiff isoforms but also by post-translational mechanisms such as protein phosphorylation. Indeed, after PKA treatment, which phosphorylates sarcomere target proteins such as titin and troponin I, passive forces were lower in the RBM20$^{E913K/+}$ patient at all measured sarcomere lengths. Although exogenous PKA decreased passive force in the RBM20$^{E913K/+}$ patient, this was not the case in the iDCM patients. Reduced phosphorylation of myofilament proteins in heart failure has been observed due to the impairment of the beta-adrenergic receptor signalling and subsequent decreased PKA activity.[31] We show that the RBM20$^{E913K/+}$ patient reacts differently to exogenous PKA than iDCM patients with respect to passive force development.

PKA-treated cells showed a clear trend towards decreased Ca^{2+}-sensitivity in RBM20$^{E913K/+}$, whereas it had no effect on control cardiomyocytes. Remarkably, Ca^{2+}-sensitivity in E913K cardiomyocytes was even lower after PKA than in control and iDCM cardiomyocytes indicating that the mutation has profound effects on both phosphorylation status and sarcomere function. Thus, apart from differences in passive tension, the E913K mutation showed a larger response to PKA with respect to calcium sensitivity compared with iDCM patients. The introduction of a negatively charged phosphate group on a protein can induce a conformational change leading to altered protein function. A possible explanation for the altered response of the RBM20$^{E913K/+}$ patient compared with IDCM might be that the additional length in the protein interferes with the induced conformational changes upon phosphorylation. If and how these additional domains interfere with conformational changes cannot be concluded from this study and additional research into this would be valuable.

The blunted FSM in E913K cardiomyocytes at baseline is in accordance with previously reported data in *Rbm20*ΔRRM mice,[7] although the effect of PKA was not investigated in these mice. The high myofilament Ca^{2+}-sensitivity and blunted FSM may contribute to disease progression in DCM. Phosphorylation of myofilament proteins can also play an important role in length-dependent activation.[32] In this study we show that the length-dependent activation was indeed impaired in the RBM20$^{E913K/+}$ patient, but was restored after exogenous PKA treatment. This indicates that in this patient, phosphorylation deficits underlie the reduced length-dependent activation and may be a secondary mutation-induced effect in disease development. Furthermore, as PKA is a downstream effector of beta-adrenergic receptor signalling, beta-blocker treatment (and thus lowering PKA activity) could be detrimental to patients with an *RBM20* mutation and its effectiveness should therefore be carefully investigated. Although missplicing of titin alone may explain the early onset and clinically aggressive *RBM20*-related DCM, we cannot exclude a contribution of missplicing of other direct RBM20 target genes that have previously been identified.[6] However, RNA binding studies revealed that *titin* mRNA was the most prominent RBM20-bound target in cardiomyocytes.[5,6] In addition, the majority of RBM20 protein was localized in nuclear aggregates that associated with *titin* mRNA.[26] Altogether, this suggests that *titin* missplicing caused by a defect in *RBM20* has a major contribution in disease onset and progression.

In conclusion, our data support a model in which haploinsufficiency of RBM20 results in more compliant titin isoforms and a disturbed FSM. In addition, we show the importance of phosphorylation on myofilament function. Although passive tension was normal and calcium sensitivity was increased at baseline, exogenous PKA could rescue the impaired FSM and unmasked decreased passive tension and decreased calcium sensitivity in the RBM20$^{E913K/+}$ patient compared with control and iDCM patients. These findings may at least in part explain the depressed contractile function in the failing heart of RBM20$^{E913K/+}$ patients. The aggressive and often malignant course of DCM caused by *RBM20* mutations underscores the importance of clinical screening for this gene and identifying the underlying pathophysiology to design possible ways of treatment.

Supplementary material

Supplementary material is available at *Cardiovascular Research* online.

Acknowledgements

We thank Dr Vasco Sequeira and Aref Najafi for technical support, Dr Jan Ruijter for statistical advice, and all previous and present members of the Pinto laboratory for helpful discussions.

Conflict of interest: none declared.

Funding

This work was supported by grants from the Netherlands Organisation for Scientific Research (NWO) (grants 825.13.007 and 836.12.002), the Netherlands Cardiovascular Research Initiative (CVON 2011-11), CVON young talent programme, EU FP7 project INHERITANCE 241924, the Lundbeck Foundation, Rembrandt grant 2013, and Arvid Nilsson's Foundation.

References

1. McNally EM, Golbus JR, Puckelwartz MJ. Genetic mutations and mechanisms in dilated cardiomyopathy. *J Clin Invest* 2013;**123**:19–26.
2. Brauch KM, Karst ML, Herron KJ, de Andrade M, Pellikka PA, Rodeheffer RJ, Michels VV, Olson TM. Mutations in ribonucleic acid binding protein gene cause familial dilated cardiomyopathy. *J Am Coll Cardiol* 2009;**54**:930–941.
3. Li D, Morales A, Gonzalez-Quintana J, Norton N, Siegfried JD, Hofmeyer M, Hershberger RE. Identification of novel mutations in RBM20 in patients with dilated cardiomyopathy. *Clin Transl Sci* 2010;**3**:90–97.
4. Haas J, Frese KS, Peil B, Kloos W, Keller A, Nietsch R, Feng Z, Muller S, Kayvanpour E, Vogel B, Sedaghat-Hamedani F, Lim WK, Zhao X, Fradkin D, Kohler D, Fischer S, Franke J, Marquart S, Barb I, Li DT, Amr A, Ehlermann P, Mereles D, Weis T, Hassel S, Kremer A, King V, Wirsz E, Isnard R, Komajda M, Serio A, Grasso M, Syrris P, Wicks E, Plagnol V, Lopes L, Gadgaard T, Eiskjaer H, Jorgensen M, Garcia-Giustiniani D, Ortiz-Genga M, Crespo-Leiro MG, Deprez RH, Christiaans I, van Rijsingen IA, Wilde AA, Waldenstrom A, Bolognesi M, Bellazzi R, Morner S, Bermejo JL, Monserrat L, Villard E, Mogensen J, Pinto YM, Charron P, Elliott P, Arbustini E, Katus HA, Meder B. Atlas of the clinical genetics of human dilated cardiomyopathy. *Eur Heart J* 2014;**36**:1123–1135.
5. Guo W, Schafer S, Greaser ML, Radke MH, Liss M, Govindarajan T, Maatz H, Schulz H, Li S, Parrish AM, Dauksaite V, Vakeel P, Klaassen S, Gerull B, Thierfelder L, Regitz-Zagrosek V, Hacker TA, Saupe KW, Dec GW, Ellinor PT, MacRae CA, Spallek B,

Fischer R, Perrot A, Ozcelik C, Saar K, Hubner N, Gotthardt M. RBM20, a gene for hereditary cardiomyopathy, regulates titin splicing. *Nat Med* 2012;**18**:766–773.
6. Maatz H, Jens M, Liss M, Schafer S, Heinig M, Kirchner M, Adami E, Rintisch C, Dauksaite V, Radke MH, Selbach M, Barton PJ, Cook SA, Rajewsky N, Gotthardt M, Landthaler M, Hubner N. RNA-binding protein RBM20 represses splicing to orchestrate cardiac pre-mRNA processing. *J Clin Invest* 2014;**124**:3419–3430.
7. Methawasin M, Hutchinson KR, Lee EJ, Smith JE III, Saripalli C, Hidalgo CG, Ottenheijm CA, Granzier H. Experimentally increasing titin compliance in a novel mouse model attenuates the Frank-Starling mechanism but has a beneficial effect on diastole. *Circulation* 2014;**129**:1924–1936.
8. Beraldi R, Li X, Martinez Fernandez A, Reyes S, Secreto F, Terzic A, Olson TM, Nelson TJ. Rbm20-deficient cardiogenesis reveals early disruption of RNA processing and sarcomere remodeling establishing a developmental etiology for dilated cardiomyopathy. *Hum Mol Genet* 2014;**23**:3779–3791.
9. Weeland CJ, van den Hoogenhof MM, Beqqali A, Creemers EE. Insights into alternative splicing of sarcomeric genes in the heart. *J Mol Cell Cardiol* 2015;**81**:107–113.
10. Chauveau C, Rowell J, Ferreiro A. A rising titan: TTN review and mutation update. *Hum Mutat* 2014;**35**:1046–1059.
11. Nagueh SF, Shah G, Wu Y, Torre-Amione G, King NM, Lahmers S, Witt CC, Becker K, Labeit S, Granzier HL. Altered titin expression, myocardial stiffness, and left ventricular function in patients with dilated cardiomyopathy. *Circulation* 2004;**110**:155–162.
12. Makarenko I, Opitz CA, Leake MC, Neagoe C, Kulke M, Gwathmey JK, del Monte F, Hajjar RJ, Linke WA. Passive stiffness changes caused by upregulation of compliant titin isoforms in human dilated cardiomyopathy hearts. *Circ Res* 2004;**95**:708–716.
13. Fukuda N, Wu Y, Farman G, Irving TC, Granzier H. Titin isoform variance and length dependence of activation in skinned bovine cardiac muscle. *J Physiol* 2003;**553**:147–154.
14. Mestroni L, Maisch B, McKenna WJ, Schwartz K, Charron P, Rocco C, Tesson F, Richter A, Wilke A, Komajda M. Guidelines for the study of familial dilated cardiomyopathies. Collaborative Research Group of the European Human and Capital Mobility Project on Familial Dilated Cardiomyopathy. *Eur Heart J* 1999;**20**:93–102.
15. Medzikovic L, Schumacher CA, Verkerk AO, van Deel ED, Wolswinkel R, van der Made I, Bleeker N, Cakici D, van den Hoogenhof MM, Meggouh F, Creemers EE, Ann Remme C, Baartscheer A, de Winter RJ, de Vries CJ, Arkenbout EK, de Waard V. Orphan nuclear receptor Nur77 affects cardiomyocyte calcium homeostasis and adverse cardiac remodelling. *Sci Rep* 2015;**5**:15404.
16. Ruijter JM, Ramakers C, Hoogaars WM, Karlen Y, Bakker O, van den Hoff MJ, Moorman AF. Amplification efficiency: linking baseline and bias in the analysis of quantitative PCR data. *Nucleic Acids Res* 2009;**37**:e45.
17. Warren CM, Krzesinski PR, Greaser ML. Vertical agarose gel electrophoresis and electroblotting of high-molecular-weight proteins. *Electrophoresis* 2003;**24**:1695–1702.
18. Ottenheijm CA, Knottnerus AM, Buck D, Luo X, Greer K, Hoying A, Labeit S, Granzier H. Tuning passive mechanics through differential splicing of titin during skeletal muscle development. *Biophys J* 2009;**97**:2277–2286.
19. van Dijk SJ, Paalberends ER, Najafi A, Michels M, Sadayappan S, Carrier L, Boontje NM, Kuster DW, van Slegtenhorst M, Dooijes D, dos Remedios C, ten Cate FJ, Stienen GJ, van der Velden J. Contractile dysfunction irrespective of the mutant protein in human hypertrophic cardiomyopathy with normal systolic function. *Circ Heart Fail* 2012;**5**:36–46.
20. van der Velden J, de Jong JW, Owen VJ, Burton PB, Stienen GJ. Effect of protein kinase A on calcium sensitivity of force and its sarcomere length dependence in human cardiomyocytes. *Cardiovasc Res* 2000;**46**:487–495.
21. Adzhubei IA, Schmidt S, Peshkin L, Ramensky VE, Gerasimova A, Bork P, Kondrashov AS, Sunyaev SR. A method and server for predicting damaging missense mutations. *Nat Methods* 2010;**7**:248–249.
22. Kumar P, Henikoff S, Ng PC. Predicting the effects of coding non-synonymous variants on protein function using the SIFT algorithm. *Nat Protoc* 2009;**4**:1073–1081.
23. Greaser ML, Warren CM, Esbona K, Guo W, Duan Y, Parrish AM, Krzesinski PR, Norman HS, Dunning S, Fitzsimons DP, Moss RL. Mutation that dramatically alters rat titin isoform expression and cardiomyocyte passive tension. *J Mol Cell Cardiol* 2008;**44**:983–991.
24. Konhilas JP, Irving TC, Wolska BM, Jweied EE, Martin AF, Solaro RJ, de Tombe PP. Troponin I in the murine myocardium: influence on length-dependent activation and interfilament spacing. *J Physiol* 2003;**547**:951–961.
25. Zhao Y, Feng Y, Zhang YM, Ding XX, Song YZ, Zhang AM, Liu L, Zhang H, Ding JH, Xia XS. Targeted next-generation sequencing of candidate genes reveals novel mutations in patients with dilated cardiomyopathy. *Int J Mol Med* 2015;**36**:1479–1486.
26. Li S, Guo W, Dewey CN, Greaser ML. Rbm20 regulates titin alternative splicing as a splicing repressor. *Nucleic Acids Res* 2013;**41**:2659–2672.
27. Long JC, Caceres JF. The SR protein family of splicing factors: master regulators of gene expression. *Biochem J* 2009;**417**:15–27.
28. Borbely A, Falcao-Pires I, van Heerebeek L, Hamdani N, Edes I, Gavina C, Leite-Moreira AF, Bronzwaer JG, Papp Z, van der Velden J, Stienen GJ, Paulus WJ. Hypophosphorylation of the Stiff N2B titin isoform raises cardiomyocyte resting tension in failing human myocardium. *Circ Res* 2009;**104**:780–786.
29. Wyles SP, Li X, Hrstka SC, Reyes S, Oommen S, Beraldi R, Edwards J, Terzic A, Olson TM, Nelson TJ. Modeling structural and functional deficiencies of RBM20 familial dilated cardiomyopathy using human induced pluripotent stem cells. *Hum Mol Genet* 2016;**25**:254–265.
30. Wyles SP, Hrstka SC, Reyes S, Terzic A, Olson TM, Nelson TJ. Pharmacological modulation of calcium homeostasis in familial dilated cardiomyopathy: an in vitro analysis from an RBM20 patient-derived iPSC model. *Clin Transl Sci* 2016;**9**:158–167.
31. Harding SE, Brown LA, Wynne DG, Davies CH, Poole-Wilson PA. Mechanisms of beta adrenoceptor desensitisation in the failing human heart. *Cardiovasc Res* 1994;**28**:1451–1460.
32. Wijnker PJ, Sequeira V, Foster DB, Li Y, Dos Remedios CG, Murphy AM, Stienen GJ, van der Velden J. Length-dependent activation is modulated by cardiac troponin I bisphosphorylation at Ser23 and Ser24 but not by Thr143 phosphorylation. *Am J Physiol Heart Circ Physiol* 2014;**306**:H1171–H1181.